# Resonance Raman Structural Evidence that the Cis-to-Trans Isomerization in Rhodopsin Occurs in Femtoseconds

**Judy E. Kim, David W. McCamant, Leyun Zhu,† and Richard A. Mathies***

*Department of Chemistry, University of California, Berkeley, California 94720*

*Received: March 31, 2000; In Final Form: September 22, 2000*

Picosecond time-resolved resonance Raman spectroscopy is used to probe the structural changes of rhodopsin's retinal chromophore as the cis-to-trans isomerization reaction occurs that initiates vision. Room-temperature resonance Raman spectra of rhodopsin's photoproduct with time delays from −0.7 to 20.8 ps are measured using 2.2 ps, 480 nm pump and 1.5 ps, 600 nm probe pulses. Hydrogen-out-of-plane (HOOP) modes at 852, 871, and 919 $cm^{-1}$, fingerprint peaks at 1272, 1236, 1211, and 1166 $cm^{-1}$, and a broad red-shifted ethylenic band at 1530 $cm^{-1}$ are present at the earliest positive pump−probe time delay of 0.8 ps, indicating that the chromophore is already in a strained, all-trans configuration. Kinetic analyses of both the HOOP and ethylenic regions of the photoproduct spectra reveal that these features grow in with fast (∼ 200 fs) and slow (∼ 2−3 ps) components. These data provide the first structural evidence that photorhodopsin has a thermally unrelaxed, torsionally strained all-trans chromophore within ∼1 ps, and possibly within 200 fs, of photon absorption. Following this ultrafast product formation, the all-trans chromophore cools and conformationally relaxes within a few picoseconds to form bathorhodopsin. This cooling process is revealed as an ethylenic frequency blue-shift of 6 $cm^{-1}$ ($\tau \sim 3.5$ ps) as well as an ethylenic width narrowing ($\tau \sim 2$ ps). The ultrafast production of photorhodopsin is likely accompanied by an impulsively driven, localized protein response. More delocalized protein modes are unable to relax on this ultrafast time scale enabling the chromophore-protein complex to store the large amounts of photon energy (30−35 kcal/mol) that are subsequently used to drive activating protein conformational changes.

## Introduction

The goal of understanding the intimate interplay between structure and function in the earliest events of protein chemistry has spurred the challenging study of time-resolved protein structural dynamics. A diverse collection of photoreactive proteins, including photosynthetic systems,[1] photoactive yellow protein,[2,3] and rhodopsins,[4−6] have been studied with both crystallographic and time-resolved spectroscopic techniques. The greatest time resolution is achieved with femtosecond electronic spectroscopy where structural information can only be inferred. To obtain a direct, real-time probe of fast protein structural changes in the physiologically relevant condensed phase, it is necessary to develop structural techniques having the highest possible time-resolution.

Time-resolved vibrational spectroscopy is a versatile tool for directly monitoring the ultrafast reaction dynamics of protein and prosthetic group structures. Both femtosecond IR[7,8] and subpicosecond Raman[9,10] spectroscopies have been used to study protein reactions. However such vibrational studies are limited to low spectral resolution because of the time-bandwidth relationship. Picosecond time-resolved resonance Raman (RR) spectroscopy allows for selective enhancement of signal from different regions of the protein with the highest combination of temporal and spectral resolution. Picosecond visible time-resolved RR with < 2 ps pulses has been used to study several proteins.[11−13] Rhodopsin, one of the more interesting photoactivated proteins, has thus far only been studied at much lower time-resolution.[14]

The visual pigment rhodopsin is a 7-α helical G-protein coupled receptor found in the membranes of retinal rod cells that contains a covalently bound 11-cis retinal protonated Schiff base chromophore. The primary event in vision, the 11-cis to all-trans isomerization of retinal, is complete in only 200 fs,[15,16] has a quantum yield of 0.67, and results in a photoproduct which stores 35 kcal/mol or 60% of the incident photon energy. The primary photoproduct of rhodopsin, photorhodopsin, has been identified by its red-shifted absorption maximum ($\lambda_{max} \sim 570$ nm)[16,17] as well as its 200 fs formation time. Photorhodopsin thermally decays to form bathorhodopsin ($\lambda_{max} \sim 540$ nm) in ∼ 5 ps.[16,18−20] Bathorhodopsin decays through a series of intermediates leading to the deprotonation of the retinal Schiff base in meta II and triggering of the G-protein cascade.

The short ground-state lifetime of photorhodopsin has prevented its definitive structural characterization. Instead, the chromophore has been inferred to be in the all-trans configuration from analogue studies.[21,22] The inability to thermally trap photorhodopsin also suggests that photorhodopsin is a hot transient which cools to form bathorhodopsin. This raises the question of which intermediate, photorhodopsin or bathorhodopsin, is the true, thermally equilibrated primary photoproduct in rhodopsin's photochemistry. The structure of room-temperature bathorhodopsin was examined with 10 and 30 ps time resolution;[14,23] these data suggest a highly distorted, all-trans chromophore structure that remains constant from 10 ps to 100 ns. Therefore, to resolve and understand the early structural events in rhodopsin photochemistry, it is necessary to obtain time-

* To whom correspondence should be addressed. E-mail: rich@zinc.cchem.berkeley.edu. Phone: (510) 642-4192. Fax: (510) 642-3599.
† Current address: Pacific Northwest National Laboratory, Richland, WA 99352.

10.1021/jp001236s CCC: $20.00 
Published on Web 01/18/2001

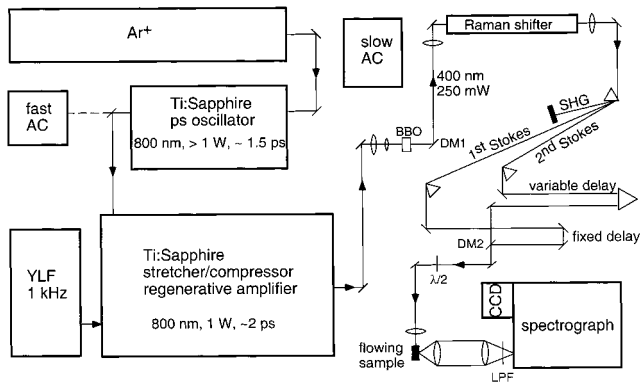


**Figure 1.** Schematic of laser apparatus for two-color pump/probe Raman experiments. AC, autocorrelator; BBO, $\beta$-barium borate crystal; DM1 and DM2, dichroic mirrors; $\lambda/2$, half-wave plate; SHG, second-harmonic light; LPF, long-pass filter; CCD, charge-coupled device detector.

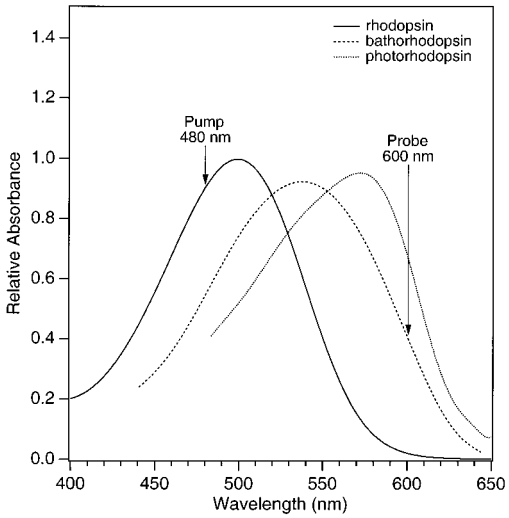


**Figure 2.** Relative absorbances of rhodopsin (solid line), bathorhodopsin (dashed line), and photorhodopsin (dotted line) at room temperature. Bathorhodopsin and photorhodopsin spectra are adapted from Kandori et al.[17] Laser wavelengths used in the two-beam, pump−probe experiments are indicated.

resolved structural snapshots of rhodopsin with the best combination of temporal (<2 ps) and spectral (<10 $cm^{-1}$) resolutions.

Here we perform time-resolved two-color RR spectroscopy to obtain structural information on the primary photoproduct in vision with the highest possible time resolution. Several key questions are addressed: What is the structure of photorhodopsin, particularly the configuration about the $C_{11}$=$C_{12}$ bond? On what time scale can we unambiguously identify the all-trans photoproduct? What changes govern the evolution of photorhodopsin to bathorhodopsin? What is the relationship between the room-temperature structure and that trapped at low-temperature? To answer these questions, we report two-color, pump−probe spectra of rhodopsin with delays from −0.7 to 20.8 ps using nearly transform-limited ps laser pulses. The results presented here help to establish a more complete picture of the mechanism of the primary photoevents in vision.

## Experimental Section

**Sample Preparation.** Rod outer segments (ROS) were isolated from bovine retinae (JA Lawson, Lincoln NE) and purified by sucrose flotation followed by sucrose density gradient centrifugation.[24] The isolated ROS were then lysed in water, solubilized in 5% Ammonyx-LO (Exciton, Dayton OH), and purified by hydroxyapatite chromatography.[25] The protein was eluted with a phosphate step gradient (30 to 150 mM $PO_4^{3-}$, pH 7) yielding ~ 12 nmol of rhodopsin/retina. The $OD_{280}/OD_{500}$ absorbance ratio was < 1.8. For the two-color experiments, separate 20 mL aliquots from a 140 mL solution (1.5 OD/cm at 500 nm) were used (150 mM $PO_4^{3-}$, 1% Ammonyx-LO, < 3 mM $NH_2OH$, with 0.25 M $NO^{3-}$ as an internal standard).

**Laser System.** The picosecond laser system and its performance characteristics were described in detail previously.[26] The setup for the current experiments is shown schematically in Figure 1. Briefly, a mode-locked ps Ti:sapphire oscillator (Spectra Physics Tsunami model 3950) was pumped with 8.5 W of the multiline visible output from an argon ion laser (Spectra Physics 2040E) to produce an 82 MHz train of low energy (~13 nJ, 1.5 ps) 800 nm pulses. These pulses were amplified by a regenerative amplifier (Spectra Physics Spitfire) pumped with 10.5 W of 527 nm light from a 1 kHz Nd:YLF laser (Spectra Physics Merlin). The resulting amplified ~ 2 ps pulses had energies of ~950 $\mu$J centered at 800 nm. These pulses were then frequency doubled to produce > 250 $\mu$J pulses at 400 nm. The doubled light was focused into a 0.5-m Raman shifter with 750 psi of $H_2$ to produce 1st Stokes (480 nm) and 2nd Stokes (600 nm) pulses which served as the pump and probe beams, respectively. The beams passed through either a variable or fixed delay before being made collinear with a dichroic beam splitter. Wavelengths used in these experiments are indicated in Figure 2 along with relative absorption spectra of rhodopsin, photorhodopsin, and bathorhodopsin. Two-color autocorrelations were 2.2 and 1.5 ps for the pump (480 nm) and probe (600 nm) pulses, respectively, and the cross correlation was 2.3 ps.

**Data Collection.** It was important to choose pump and probe wavelengths which minimized detected fluorescence while maximizing resonance enhancement of the photoproduct. Three sets of pump/probe wavelengths were explored: 458 nm pump/566 nm probe (oscillator $\lambda$ = 770 nm), 480 nm pump/600 nm probe (oscillator $\lambda$ = 800 nm), and 500 nm pump/633 nm probe (oscillator $\lambda$ = 830 nm). The pump and probe powers were set such that the photoalteration parameter[27] for rhodopsin $F_{rho}$ was equivalent for each pump wavelength, and $F_{batho}$ was equivalent for each probe wavelength. For a time delay of 20 ps the best S/N was obtained with the 480 nm pump/600 nm probe combination.

Raman scattering was generated by focusing the 480 nm pump and 600 nm probe laser beams into the center of a 2 mm i.d. square capillary using a 50 mm spherical lens. Spot sizes were 90 × 65 $\mu$m for the pump beam and 75 × 75 $\mu$m for the probe beam. The sample was flowed from an ice cooled reservoir at a rate of ~ 18 cm/s to ensure that each laser pulse interrogated fresh sample. The conversion of rhodopsin to photoproduct by the laser beam can be approximated from the photoalteration parameter[27] $F = (3.82 \times 10^{-21} E\phi\epsilon)/A$ where $E$ is the number of photons per pulse, $\phi$ is the quantum yield for the photoreaction, $\epsilon$ is the decadic extinction coefficient, and $A$ is the beam area. The 480 nm pump pulse energy of 200 nJ ($F_{rho}$ ~ 1) was chosen to maximize photolysis of rhodopsin while avoiding saturation effects. The photoproduct signal for a time delay of 20 ps was found to increase linearly with pump power. The 600 nm probe pulse energy was 410 nJ, resulting in $F_{rho}$ <0.1 ($\epsilon_{rho}$ = 812 $cm^{-1}$ $M^{-1}$) and $F_{batho}$ ~ 0.8 (using $\epsilon_{batho}$ = 14990 $cm^{-1}$ $M^{-1}$, $\phi$ = 0.5). Scattering in a 20 ps delay photoproduct spectrum increased linearly in response to a 2-fold increase in probe power, and the spectra were identical.

The Raman scattering was collected by a 5 cm focal length collection lens (f/1) and then focused by a 20 mm focal length lens onto the entrance slit of a single-stage f/4 spectrograph (Spex 500 M). The spectrograph was equipped with a 1200 grooves/mm grating blazed at 500 nm and had a spectral bandwidth of 11.5 $cm^{-1}$ (300 $\mu$m slits). A long-pass filter (Corning 2-61) was placed in front of the entrance slit to reject Rayleigh scattering. The spectrally dispersed light was detected by a $LN_2$ cooled CCD detector (Princeton Instruments LN/CCD 1152). Frequencies were calibrated by comparison with the Raman spectrum of cyclohexane and a neon emission spectrum. Reported frequencies are accurate to $\pm$ 2 $cm^{-1}$. A white light spectrum was also recorded to correct for spectral sensitivity of the detection system.

For each time delay, three sets of data were acquired: pump + probe, probe-only, and pump-only. First, alternating pump + probe and probe-only data were continuously recorded at 5 min intervals until $\sim$ 30% of the bulk sample was bleached. The total acquisition time resulting in this bleach was 80 min (40 min for pump + probe and 40 min for the probe-only spectral data sets). Aside from overall peak intensity decreases due to decreasing rhodopsin concentration and general rise in fluorescent background as the sample bleached, no spectral changes were observed throughout the 40 min of data collection. The rise in background emission as the sample is bleached has been well documented[28] and is due to oxidized membrane lipids, retinal oxime, or bleached and denatured protein. A pump-only spectrum (40 min) was then recorded. Following this, pump + probe, probe-only, and pump-only spectra (40 min each) of completely bleached sample with no internal standard, and of just 0.25-M nitrate were recorded. It was necessary to record spectra of bleached sample and nitrate solution separately since the presence of nitrate caused bleached opsin to precipitate.

**Temporal and Spectral Deconvolution.** The observed signal $S(t)$ is the convolution of the instrument response $G(t)$ with the molecular response $R(t)$. The instrument response is a Gaussian distribution with full-width at half-maximum ($\tau_{fwhm}$) of 2.3 ps:

$$G(t) = \sqrt{\frac{4(\ln 2)}{\pi\tau_{fwhm}^2}}\exp\left(\frac{4(\ln 2)t^2}{\tau_{fwhm}^2}\right) \qquad (1)$$

The molecular response function $R(t)$ is expected to consist of components reflecting formation and relaxation of photoproduct. Therefore, $R(t)$ was chosen to be the sum of an error function and an exponential growth:

$$R(t) = A\left[\frac{1}{2}\mathrm{erf}\left(\frac{(t-\tau_{step})2\sqrt{\ln 2}}{\sigma_{fwhm}}\right)+\frac{1}{2}\right] + B\left[1-\exp\left(-\frac{(t-\tau_{step})}{\tau_{exp}}\right)\right] \quad \text{for } t > 0, \text{ and}$$

$$R(t) = 0 \text{ for } t \le 0 \qquad (2)$$

The error function is a step function at $\tau_{step}$ convolved with a normal distribution of width $\sigma_{fwhm}$. $\tau_{step}$ represents the average time delay between absorption of a photon and product formation. The slow exponential growth with time constant $\tau_{exp}$ accounts for subsequent relaxation in the photoproduct ground state. The growth of photoproduct signal was modeled by fixing the instrument response and $\sigma_{fwhm}$ while varying the parameters $A$, $B$, $\tau_{step}$, and $\tau_{exp}$ of the molecular response function to obtain the best least-squares fit of $S(t)$ to the data. Other molecular response functions, such as single exponential, were also tried but produced inferior fits compared to $R(t)$. Single exponential rise functions were unable to simultaneously fit both the long-time data and the fast rise at early times (0.8 ps).

When the pump and probe pulses overlap temporally, it is necessary to determine the average time after production that the photoproduct scatters a Raman photon. At positive time delays (probe pulse arrives after the pump pulse), some of the molecules will be probed prior to being pumped. At negative nominal pump−probe time delays ($\Delta t_{pulse} < 0$), only the portion of the time delay distribution lying at positive times will give rise to photoproduct signal. To find the average time *after pumping* that molecules are probed, it is necessary to look at the distribution of *positive* time delays. The calculated average positive time delay $\langle \Delta t > 0 \rangle$ between pump and probe events for two pulses separated by $\Delta t_{pulse}$ and with cross correlation $G(t)$ is given by

$$\langle \Delta t > 0 \rangle = \frac{\int_0^\infty tG(t-\Delta t_{pulse})dt}{\int_0^\infty G(t-\Delta t_{pulse})dt} \qquad (3)$$

The data points with time delays greater than 2.3 ps are unaffected by this correction, but the average positive time delay values for pulse delays of −0.7 and 0.8 ps were +0.6 ps and +1.2 ps, respectively.

The photoproduct spectra were also spectrally deconvolved from the instrument response function in order to isolate individual line intensities. The intrinsic molecular photoproduct peaks were assumed to be the same as those in the low-temperature bathorhodopsin spectrum.[29] The overall instrument response was experimentally measured by recording a probe laser spectrum with monochromator slits open to 300 $\mu$m.

## Results

To reveal Raman spectra of the photoproduct, it was necessary to remove any broad features in the pump + probe spectra due to the pump pulse as well as signal due to unphotolyzed rhodopsin and/or bleached sample. First, corresponding bleach spectra were subtracted from all pump + probe, probe-only, and pump-only spectra. As an example, Figure 3 shows (A) rhodopsin probe-only minus bleach, (B) rhodopsin pump + probe minus bleach, and (C) rhodopsin pump-only minus bleach spectra for a 20.8 ps delay between pump and probe pulses. Negative counts are due to the increased fluorescence inherent to the 100% bleached sample. The pump-only spectrum was subtracted from all pump + probe spectra and any remaining broad backgrounds were removed with spline fits, resulting in photolysis spectra consisting of scattering from rhodopsin, photoproduct, and the nitrate internal standard (spectrum D). All such photolysis spectra having time delays from −0.7 to 20.8 ps are presented in Figure 4. To obtain accurate kinetic information, the photolysis spectra were normalized for variations in pump and probe powers during the experiment. The fluorescence background served as an indicator of pump power variation while the intensity of the 1048 $cm^{-1}$ nitrate peak served as an internal standard for probe power.

Difference spectra were obtained by subtracting a fraction of the normalized probe-only spectrum from the normalized photolysis spectrum such that the 970 $cm^{-1}$ mode of rhodopsin disappeared. This procedure had no significant effect on the features of the photoproduct spectrum even for variations in the subtraction coefficient up to 10%. For the 20.8 ps delay example in the bottom part of Figure 3, 0.45 × (probe-only) spectrum was subtracted from the photolysis spectrum (D) to

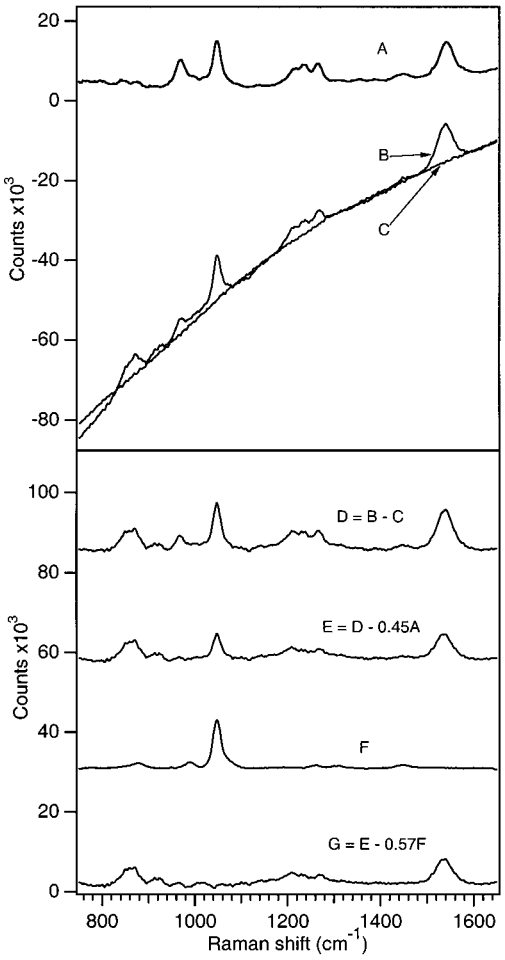


**Figure 3.** Two-color data reduction procedure using 20.8 ps delay spectra as an example. Top part. Spectrum (A) is the probe-only minus bleach, spectrum (B) is pump + probe minus bleach, (C) is pump-only minus bleach. Negative counts are a consequence of the bleach spectra having higher background levels than corresponding unbleached spectra. Bottom part. Spectrum (D), the photolysis spectrum, is pump + probe (B) minus pump-only (C). A fraction of the probe-only spectrum (A) is then subtracted from this photolysis spectrum to yield a difference spectrum (E). To remove scattering due to nitrate, a fraction of the 0.25-M nitrate spectrum (F) is subtracted to yield a difference spectrum consisting of just the photoproduct (G). All spectra in the bottom part were background-corrected for broad fluorescent backgrounds using spline fits.

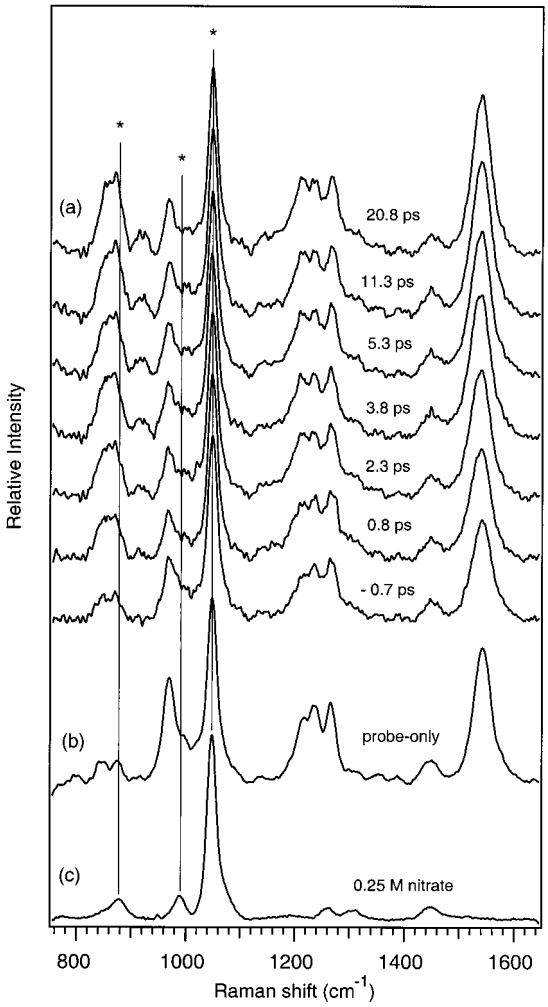


**Figure 4.** (a) Two-color pump + probe time-resolved resonance Raman photolysis spectra of the rhodopsin to bathorhodopsin transition using 480 nm pump (200 nJ) and 600 nm probe (410 nJ) pulses. Peaks indicated by the asterisk are due to nitrate. The buffered rhodopsin solution had a starting OD of 1.5/cm at 500 nm and consisted of 150 mM $PO_4^{3-}$ with 1% Ammonyx-LO, < 3 mM $NH_2OH$, and 0.25-M $NO_3^-$. (b) Probe-only (600 nm) rhodopsin spectrum. (c) Nitrate spectrum (0.25-M $NO_3^-$, 150 mM $PO_4^{3-}$, 1% Ammonyx-LO and < 3 mM $NH_2OH$).

yield a spectrum consisting of photoproduct and internal standard (E). Since the rhodopsin sample contains the nitrate standard, this process removed 45% of the nitrate scattering as well. Remaining peaks due to nitrate were removed from the difference spectrum by subtracting the necessary fraction (0.57) of the 0.25-M nitrate spectrum (F) from the difference spectrum (E) to produce spectrum (G). Rhodopsin subtraction coefficients for all time delays were consistent with the experimentally observed bulk bleach rate and the sum of subtraction coefficients for rhodopsin and nitrate removal was close to unity, as expected. Difference spectra for all time delays (−0.7 to 20.8 ps) are presented in Figure 5.

The difference spectra at all but the earliest time delay clearly exhibit vibrational features of a distorted all-trans retinal chromophore structure,[30] with peaks at ∼1530−1535, 1272, 1236, 1211, 1166, 1019, 1005, 965, 919, 871, and 852 $cm^{-1}$. At the nominally negative time delay of −0.7 ps, a broad red-shifted ethylenic and an unresolved band of hydrogen-out-of-plane (HOOP) modes from 800 to 880 $cm^{-1}$ characteristic of bathorhodopsin have already appeared. By 0.8 ps the fingerprint region with lines at 1166, 1211, 1236, and 1272 $cm^{-1}$ becomes discernible as well; the frequencies in this region remain constant to 20.8 ps and the relative intensities are unchanged after ∼2.3 ps. HOOP modes at 852, 871, and 919 $cm^{-1}$ also appear by 0.8 ps; these modes continue to grow in intensity until ∼3.8 ps while their frequencies are unchanged. The 871 $cm^{-1}$ mode continues to grow until ∼11.3 ps (see below).

Kinetic analyses were performed on the ethylenic and HOOP peaks. The rise of the ethylenic peak intensity after photolysis is plotted in the upper part of Figure 6. The system response was deconvolved from the experimental data points, yielding a modeled molecular response consisting of fast product formation (expressed as an error function) and slow molecular relaxation (expressed as an exponential function) components in the form of eq 2. It was determined that 75% of the signal is due to the fast component and 25% is due to the slow component. We see that the time constants for ethylenic growth are $\tau_{step} = 110 \pm 90$ fs and $\tau_{exp} = 2.3 \pm 1.7$ ps. The appearance of overall HOOP intensity (815−940 $cm^{-1}$) is plotted in the bottom part of Figure 6. Upon deconvolving the cross-correlation as described above, it was determined that 58% of the signal is

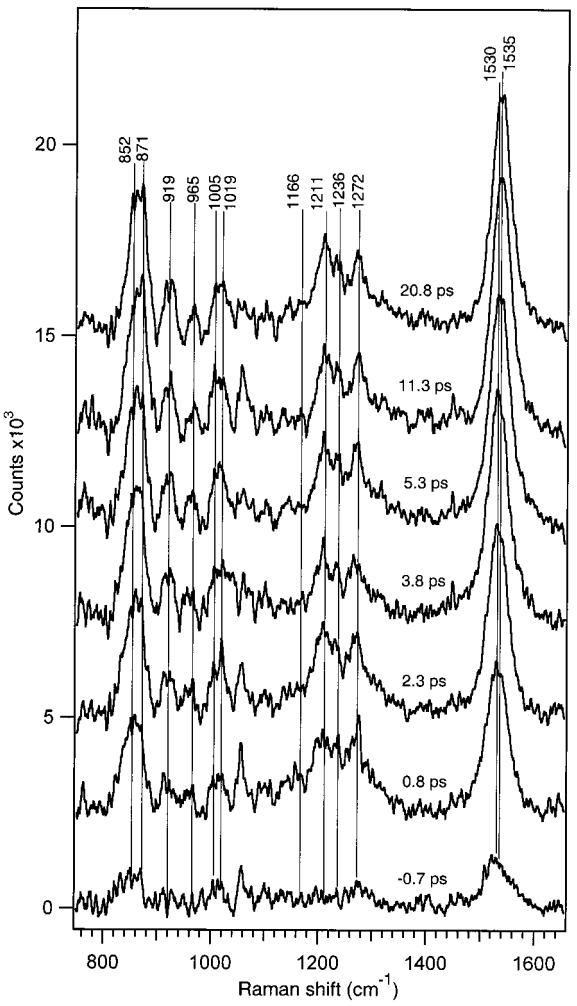


**Figure 5.** Two-color time-resolved resonance Raman difference spectra of photorhodopsin and bathorhodopsin at room temperature. The pump and probe wavelengths and powers as well as sample conditions are the same as in Figure 4.

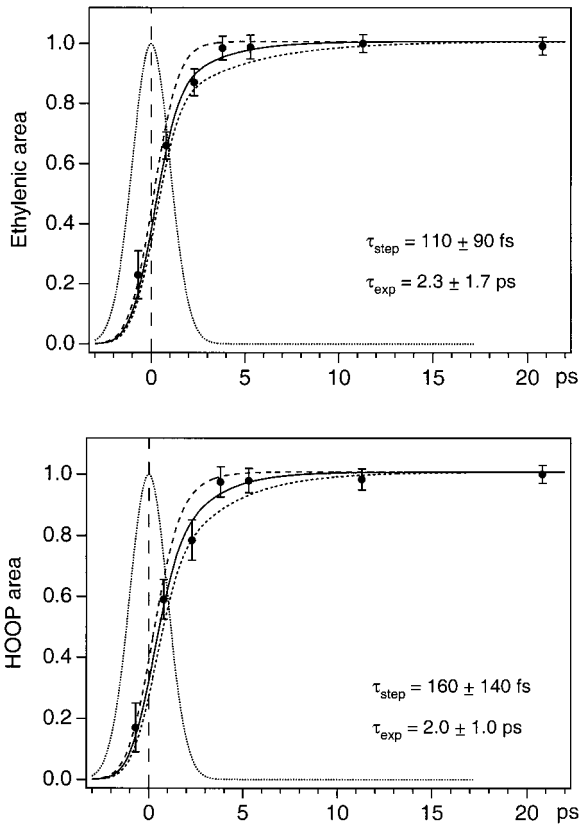


**Figure 6.** Kinetic appearance of photoproduct lines as a function of time delay. Top (●) Ethylenic areas are presented along with a least-squares fit for the convolution of the laser cross-correlation with the function in eq 2, yielding parameter values of $A = 0.75$, $B = 0.25$, $\sigma_{fwhm} = 50$ fs, $\tau_{step} = 110 \pm 90$ fs, and $\tau_{exp} = 2.3 \pm 1.7$ ps. The dashed lines indicate the fit at the 95% confidence limit using $\tau_{step} = 200$ fs, $\tau_{exp} = 4.0$ ps and $\tau_{step} = 20$ fs, $\tau_{exp} = 0.7$ ps with A, B, and $\sigma_{fwhm}$ unchanged. Bottom (●) HOOP (815−940 cm$^{-1}$) areas are presented along with a temporal convolution of the laser cross-correlation with the same function as above, yielding best fit parameters of $A = 0.58$, $B = 0.42$, fwhm = 50 fs, $\tau_{step} = 160 \pm 140$ fs and $\tau_{exp} = 2.0 \pm 1.0$ ps. Dashed lines indicate the fit at the 95% confidence limit using $\tau_{step} = 200$ fs, $\tau_{exp} = 4.0$ ps and $\tau_{step} = 20$ fs, $\tau_{exp} = 0.7$ ps with A, B, and $\sigma_{fwhm}$ unchanged. The dotted lines indicate the laser cross correlation.

due to a fast component ($\tau_{step} = 160 \pm 140$ fs, $\sigma_{fwhm} = 50$ fs) while 42% is due to a slow component ($\tau_{exp} = 2.0 \pm 1.0$ ps). The dashed lines in Figure 6 indicate the 95% confidence intervals.

To examine the frequency and shape changes of the ethylenic band, we deconvolved the instrument response from the experimental result to reveal the true ethylenic peak shape (Figure 7). The earliest time ( −0.7 ps) ethylenic band has a frequency of 1530 cm$^{-1}$ and this mode shifts to 1536 cm$^{-1}$ by 11.3 ps, where it remains unchanged at 20.8 ps. The width of the peak also shifts from 35 to 30 cm$^{-1}$ by 20.8 ps. Plots of the deconvolved C═C frequency and width vs average positive time delays are shown in the top and middle parts of Figure 8 along with the corresponding low-temperature values for comparison. These data were fit to a single exponential, yielding C═C frequency and width shift times of 3.5 ± 1.0 and 2.2 ± 1.0 ps, respectively.

To investigate the changes in relative intensity of the overlapping 852 and 871 cm$^{-1}$ photoproduct HOOP modes, it was necessary to decompose as well as deconvolve these bands. Since the spectral resolution prevents us from experimentally determining the HOOP frequencies accurately, we assume the intrinsic peak positions and widths stay constant and are identical to the low temperature (and >10 ps room temperature) values of 852 and 871 cm$^{-1}$ with fwhm of 16 and 10 cm$^{-1}$, respectively (dotted curves in Figure 9).[29] The low-temperature basis spectra were convolved with the instrument response and resulted in the broad peaks at 852 and 871 cm$^{-1}$ with fwhm of 33 and 30 cm$^{-1}$, respectively (dashed curves in Figure 9). The sum of these broad peaks is shown as the solid curve in Figure 9. The ratio of the relative intensities ($I_{871}/I_{852}$) as a function of time delay is plotted in the bottom part of Figure 8. This ratio approaches the low-temperature value with a time constant of $\tau = 3.5 \pm 1.0$ ps. The intensity of the HOOP peak at 920 cm$^{-1}$ was fit using the same procedure.

## Discussion

The spectra presented here provide the earliest structural snapshots of the photochemistry of vision as well as new insight into the structure and kinetics of the earliest photointermediates. The structural changes involved in the transition from rhodopsin to photorhodopsin, and from photorhodopsin to bathorhodopsin are described for the first time. In addition, the similarity of the room-temperature photoproduct vibrational structure to that of the low-temperature species revealed here has profound implications for the energy storage mechanism in the primary event.

**Photorhodopsin Formation Time**. Raman spectra of the primary photoproduct, photorhodopsin, are recorded at our

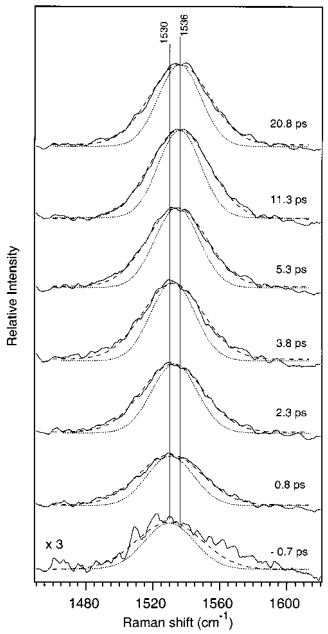


**Figure 7.** Deconvolution of the ethylenic regions of the photoproduct spectra from Figure 5. The raw data and a Gaussian fit to the raw data are indicated by the solid and dashed lines, respectively. The dotted line is the deconvolved ethylenic line.

earliest time delay. The appearance of photorhodopsin is best modeled as the sum of two kinetic components, yielding fast time constants of 110 ± 90 and 160 ± 140 fs for the growth in the ethylenic and HOOP regions, respectively. Although the error limits are understandably large, the ultrafast formation times derived in our time-resolved structural experiments are identical to the 200 fs appearance time previously obtained from femtosecond transient absorption experiments.[15,16] The previous experiments were interpreted in terms of a barrierless transition on nonadiabatic potential energy surfaces as would be expected for a Landau−Zener (LZ) tunneling mechanism on a one-dimensional cis-trans reaction coordinate. This LZ model predicts that there is a direct correlation between the quantum yield $\phi$ and the nuclear velocity $v$ along the reaction coordinate; this relationship between $\phi$ and $v$ was subsequently established in experiments with rhodopsin containing retinal analogues.[31−33]

More recent ab initio calculations on truncated five-carbon protonated Schiff bases (PSB) have explored the multidimensional nature of the isomerization coordinate.[34−36] The cis to trans isomerization coordinate consists of three coupled modes: the torsional motion about the central double bond, the symmetric stretching of the retinal chain center, and the in-phase stretching of the ethylenic and Schiff base bonds. The calculations illustrated the presence of a conical intersection which allows for a barrierless and highly efficient $S_1$ to $S_0$ decay channel and is fully consistent with the observed speed of the isomerization reaction. Methylation of one of the carbons in this PSB model led to a 2-fold increase in the slope of $S_1$, further corroborating experimental results which directly link the reaction speed to nonbonded interactions between the $C_{13}-CH_3$ and $C_{10}-H$ groups.[31,32] The predicted lack of excited-state equilibration was also consistent with the observation of coherent vibrational motion along low-frequency torsional modes in the photoproduct.[37] In a study of a longer ten-carbon PSB, an energy plateau on the $S_1$ surface was calculated, thus decreasing the isomerization rate.[36] It was suggested that an important role of the protein is to remove this energy plateau from the $S_1$ potential resulting in the observed ballistic motion of the wave packet to the ground-state photoproduct well.

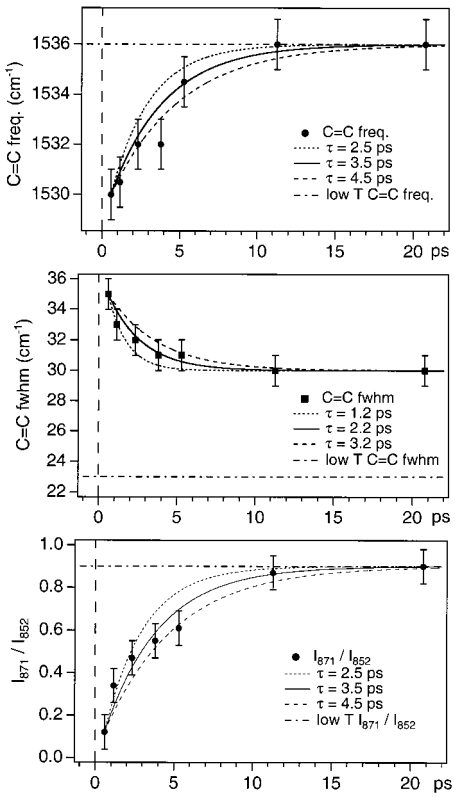


**Figure 8.** Top. (●) Plot of photoproduct ethylenic frequency as a function of time delay. Single-exponential functions with $\tau = 2.5$ ps (···), $\tau = 3.5$ ps (—) and $\tau = 4.5$ ps (- - -) are also shown. The 77 K bathorhodopsin C═C frequency is also indicated (dashed−dotted line). Middle. (■) Plot of photoproduct ethylenic width as a function of delay time. Single-exponential functions with $\tau = 1.2$ ps (···), $\tau = 2.2$ ps (—) and $\tau = 3.2$ ps (- - -) are also shown. The 77 K bathorhodopsin C═C width is also indicated (dashed−dotted line). Bottom. (●) Plot of the ratio $I_{871}/I_{852}$ of photoproduct HOOP lines as a function of average positive time delay. Single-exponential functions with $\tau = 2.5$ ps (···), $\tau = 3.5$ ps (—) and $\tau = 4.5$ ps (- - -) are shown. The 77 K bathorhodopsin $I_{871}/I_{852}$ ratio is also indicated (dashed−dotted line).

**Structure of Photorhodopsin.** The ultrafast production time of photorhodopsin and its subsequent picosecond decay to bathorhodopsin have made it very difficult to obtain structural information on this primary photoproduct. The photorhodopsin to bathorhodopsin transition is thought to occur in ∼3−9 ps,[16,18−20] but the molecular identity of photorhodopsin was unresolved. Our difference spectra with $\Delta t_{pulse} \leq 3$ ps spectra provide the first structural characterization of photorhodopsin. Figure 10 presents the Raman spectra of rhodopsin and photorhodopsin along with normal mode assignments. Our difference spectra show that within ∼2 ps of photon absorption, the following vibrational changes occur: the ethylenic peak shifts from 1544 to 1530 $cm^{-1}$; the $C_{10}-C_{11}$ single bond fingerprint mode shifts from 1097 to 1166 $cm^{-1}$; the $C_{14}-C_{15}$ stretch shifts from 1190 to 1211 $cm^{-1}$, the $C_{12}-C_{13}$ shifts from 1234 to 1236 $cm^{-1}$; and HOOP modes appear at 852, 871, and 919 $cm^{-1}$. In fact, the two-pulse modeling suggests that the photorhodopsin HOOP peaks and the red-shifted ethylenic band are already present by ∼200 fs. The frequency increase of the C−C stretches and the corresponding frequency decrease of the ethylenic band relative to rhodopsin are consistent with the more delocalized electronic structure of the red-absorbing photorhodopsin chromophore.[38] The intensities and frequencies of the strong HOOP modes are *identical* to those found in bathorhodopsin trapped at 77 K which is known to contain an all-trans chromophore.[39,40] This fact together with the observation

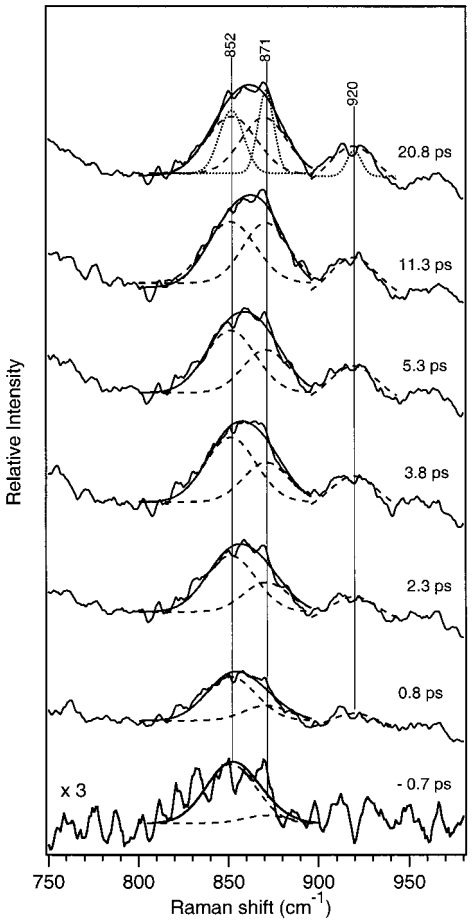


**Figure 9.** Deconvolution and decomposition of the photoproduct HOOP intensities. The best fit to the experimental data is indicated by the solid line and the individual convolved HOOP components that were summed to achieve the best fit are indicated by the dotted lines. The low-temperature photoproduct peaks at 852, 871, and 920 $cm^{-1}$ used as basis spectra are indicated by the dotted lines in the 20.8 ps spectrum.

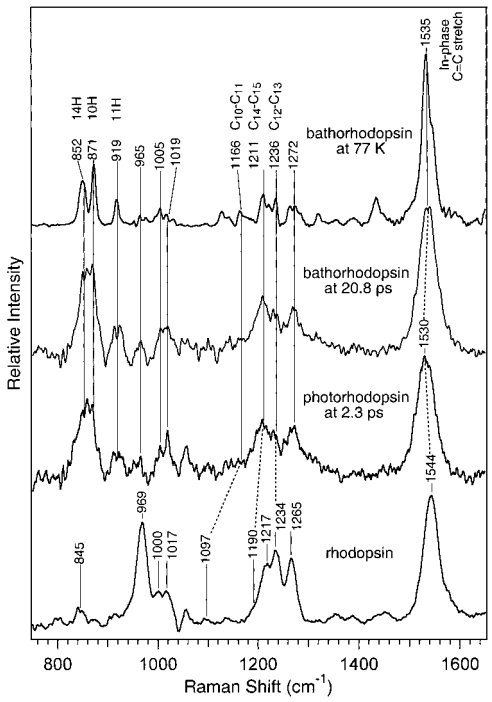


**Figure 10.** Two-color, time-resolved resonance Raman spectra of photorhodopsin (2.3 ps spectrum) and bathorhodopsin (20.8 ps spectrum) at room-temperature. For comparison the RR spectra of room-temperature rhodopsin and of the photoproduct trapped at 77 K are also presented.[29] Normal mode assignments are taken from Palings et al.[24,42]

that these room-temperature HOOP modes remain unchanged throughout our range of time delays from 0.8 to 20.8 ps provides evidence that the chromophore of photorhodopsin has an all-trans configuration about the $C_{11}$=$C_{12}$ bond even within the first ~200 femtoseconds following photon absorption. This result casts doubt on the earlier suggestion based on a study of an 11-cis locked rhodopsin analogue that the formation of photorhodopsin does not involve an isomerization about the $C_{11}$=$C_{12}$ bond[41] as well as the possibility that photorhodopsin is an excited-state transient.[20]

One of the most interesting aspects of the room-temperature structure of photorhodopsin is the presence of HOOP modes at 852, 871, and 919 $cm^{-1}$. These peaks have also been observed in other room-temperature studies of bathorhodopsin[14,23] but are not present in the all-trans PSB spectrum.[30] These unusually intense peaks also appear in the low-temperature spectrum of bathorhodopsin and have been assigned as the $C_{14}$−H (852 $cm^{-1}$), $C_{10}$−H (871 $cm^{-1}$), and $C_{11}$−H (920 $cm^{-1}$) HOOP modes.[39,42] It was determined that the 852 and 871 $cm^{-1}$ modes gain significant intensity in the all-trans photoproduct due to twists primarily about polyene chain single bonds that produce a partial pyramidalization of the indicated carbon centers.[40] Such twisting is also consistent with the observed spectral red-shift of photorhodopsin.[43] The presence of the isolated $C_{11}$−H wagging mode at 919 $cm^{-1}$ is consistent with Raman[39] and NMR[44] studies on low-temperature bathorhodopsin, indicating that there is a perturbation near the center of the retinal chain that uncouples the $C_{11}$−H and $C_{12}$−H wags and possibly contributes to chain distortions.[39] The origin of this uncoupling will be discussed below.

Our structural characterization of photorhodopsin is further supported by theoretical calculations. Car-Parrinello ab initio molecular dynamics studies indicate the formation of intense HOOP modes as the chromophore moves from the transition state to the photoproduct ground state.[45,46] A soliton-like, coherent charge propagation is predicted to accompany the cis to trans isomerization. The charge transport is strongly coupled to out-of-plane oscillations in the chromophore, thereby giving rise to intense HOOP modes. The presence of these modes indicates a high degree of chain distortion[47] that is relevant for energy storage.

**Photorhodopsin to Bathorhodopsin Transition.** Our picosecond time-resolved resonance Raman difference spectra of the photoproduct are the first measurements of the structural changes accompanying the photorhodopsin to bathorhodopsin transition. We believe that this transition occurs in a few picoseconds and is dominated by chromophore cooling and some minor conformational relaxation, suggesting that *bathorhodopsin is the first true, thermally equilibrated intermediate in the photochemistry of vision.* There are several observations that support this claim: (1) the shift in ethylenic frequency from 1530 to 1536 $cm^{-1}$ with $\tau = 3.5 \pm 1$ ps, (2) the decrease in ethylenic width from 35 to 30 $cm^{-1}$ in $2.2 \pm 1$ ps, (3) the overall increase in photoproduct ethylenic ($\tau = 2.3 \pm 1.7$ ps) and HOOP ($\tau = 2.0 \pm 1$ ps) peak intensities, and (4) the differential rise in the 871 $cm^{-1}$ peak relative to the 852 $cm^{-1}$ peak ($\tau = 3.5 \pm 1$ ps).

The first three observations and their time scales are fully consistent with chromophore cooling, most likely through intramolecular vibrational redistribution (IVR). The time de-

pendent changes of the ethylenic frequency and width can be understood in terms of the heterogeneous population of high-lying vibrational levels in the anharmonic ground-state well and their relaxation. Excess thermal energy remains localized in the Franck−Condon (FC) modes immediately after excitation and photochemistry, causing the temperature of these modes to be high; consequently a large inhomogeneous distribution of C═C frequencies is observed. Subsequent IVR depopulates the high-lying levels, causing the observed blue-shift and narrowing of the ethylenic peak. Such frequency and width changes were observed, for example, in the cooling of heme in carbonmonoxy myoglobin[12] and following the photochemical hydrogen migration in cycloheptatrienes.[48] Raman intensity changes are also expected to appear as a result of molecular thermalization. Stokes resonance Raman scattering is highly sensitive to the degree of vibrational excitation; specifically, there is an increase in scattering with a decrease in temperature.[49] A bacteriorhodopsin (bR) molecule whose excess vibrational excitation is localized in the FC modes (before any IVR or vibrational cooling has occurred) will have an ethylenic Raman cross section that is $\sim$ 40% of the value for a totally thermalized, cool molecule.[49] In the current experiment, Raman signals of the ethylenic and HOOP modes at the earliest average positive time delay of 0.6 ps are 75% and 58% of the values at the longest delay of 20.8 ps, respectively. Since some relaxation has most likely occurred within the first 0.6 ps, these measured values are reasonable and fall within the limit established above for bR. Therefore, the observed increase in overall Stokes intensities strongly supports the idea that photorhodopsin's decay is largely due to chromophore thermalization. Finally, the observed time scales for the C═C blue-shift, C═C width narrowing and overall intensity increases are also consistent with photorhodopsin cooling. Anti-Stokes Raman spectra of bR revealed a $3 \pm 1$ ps time constant for IVR.[11,49] This time constant is remarkably similar to the $\sim$ 2−3.5 ps constant obtained in the current experiment and further implicates IVR as the main pathway to bathorhodopsin.

Nevertheless a component of the transition to bathorhodopsin involves some conformational relaxation of the chromophore as it adjusts to the protein binding pocket. The HOOP intensities are sensitive to this conformational relaxation as indicated by the shift of the 871/852 $cm^{-1}$ intensity ratio to the low-temperature value with a time constant of $3.5 \pm 1$ ps. It appears that the protein environment causes the hot, all-trans photorhodopsin chromophore to distort in order to minimize steric interaction with residues as it cools to form bathorhodopsin, resulting in a change in the relative conformational distortion and concomitantly a change in relative HOOP intensities.

Aside from a general intensity increase, the 920 $cm^{-1}$ $C_{11}$−H HOOP mode frequency remains constant during the photorhodopsin to bathorhodopsin transition. This indicates that the appearance of bathorhodopsin does not involve changes in the interaction of Glu113 with the center of the retinal chain. In all-trans retinal and in rhodopsin, the $C_{11}$ and $C_{12}$−H wags are strongly coupled to produce a combination HOOP mode near 960−970 $cm^{-1}$. In native low- and room-temperature bathorhodopsin, however, an isolated $C_{11}$−H HOOP is observed at 920 $cm^{-1}$. This uncoupling of the $C_{11}$−H and $C_{12}$−H wags requires a perturbation near the center of the retinal chain that results in a reduced $C_{12}$−H wag force constant as well as a reduced coupling of the $C_{11}$−H with the $C_{12}$−H wag.[42] NMR data on the low-temperature bathorhodopsin chromophore and semiempirical molecular orbital calculations have shown that the Glu113 counterion is located $\sim$3 Å from the $C_{12}$ position, suggesting a possible mechanism for the $C_{11}$−H and $C_{12}$−H wag uncoupling.[50] Any change in the interaction between Glu113 and the retinal chain center should affect the reduced $C_{11}$−H and $C_{12}$−H coupling constant and manifest itself as an evolution of the 920 $cm^{-1}$ $C_{11}$ HOOP mode. Within our S/N, the position of this mode remains unchanged throughout the experiment. We thus conclude that the formation of bathorhodopsin from photorhodopsin does not involve altered Glu113-retinal interactions.

**Protein Response and Energy Storage.** Protein response to the isomerization reaction in rhodopsin consists of first a local impulsive structural rearrangement that is driven by the ballistic motion of chromophore isomerization followed by a slower, thermally activated, diffusive motion that allows for more global energy redistribution within the chromophore-protein complex. In drawing these conclusions we rely upon the chromophore structure in the photoproduct as a probe of protein structure and structural changes. This analysis is justified because in this system, protein−chromophore interactions are close and highly specific: (i) An exact positioning of the chromophore relative to the dipolar and charged residues in the binding pocket determines the opsin shift,[51] (ii) The presence of a unique binding pocket is further illustrated by the enantioselective binding of the chromophore,[52] and (iii) Intimate protein−chromophore interactions during the isomerization process itself are evidenced by decreases in reaction rate and quantum yield accompanying modification of the chromophore structure.[31,32] Since the protein provides a well-defined and specific "solvent cage" around the chromophore, the chromophore vibrational structure can be used as a probe of the protein binding pocket environment and its structural changes.

Our observation that the room-temperature bathorhodopsin vibrational structure at <1 ps time delay (before IVR has occurred) is nearly identical to that of the low-temperature trapped species which contains a strained all-trans chromophore suggests that the binding pocket changes accompanying the isomerization have occurred before energy has been redistributed within the chromophore itself or to the surrounding protein. In addition, since the isomerization reaction is known to occur at temperatures as low as 4 K,[53,54] thermal energy can also be excluded as the driving force for immediate protein changes accompanying isomerization. This suggests that the immediate protein response consists of a localized nonrandom movement of binding pocket residues and perhaps water molecules due to impulsive interaction with the ballistic motion of the isomerizing chromophore. This impulsive response to photoisomerization is analogous to the sub-100 fs inertial response observed in the light harvesting proteins of cyanobacteria which is thought to arise from librational motions of amino acid residues or water molecules in the chromophore binding site.[55,56] We believe that the immediate protein response resulting from photon absorption is unlike random protein motion in that these reaction-driven motions are highly energetic and there is likely to be coherence among several of these reaction-driven protein modes. For rhodopsin it is reasonable to expect an inertial protein response localized primarily in the region near $C_{11}$═$C_{12}$ where the largest NMR differences upon isomerization are observed.[44] This analysis also suggests that the changes observed in low-temperature (77 K) FTIR, including alterations in the peptide backbone, water molecules, and some amino acid residues,[57−61] are caused by these barrierless inertial motions as the rhodopsin chromophore isomerizes and collides with nearby protein residues. Given that most FTIR spectral changes can be attributed to changes in weak bonds, e.g., hydrogen bonds,[60−62]

the highly energetic chromophore should be able to impulsively drive through any barriers along these degrees of freedom.

The highly strained, all-trans chromophore of bathorhodopsin remains unchanged over the time range of ~20 ps, indicating that there is essentially no protein relaxation affecting the energy of the protein−chromophore complex on this time scale. In fact, it has been suggested that the bathorhodopsin chromophore is unaltered out to 100 ns after formation.[23] Therefore, after the fast, impulsively driven inertial component of the protein response, subsequent protein response affecting chromophore structure appears to be much slower (> 20 ps and possibly 100 ns). Such a large separation of time scales for binding pocket motion has been observed in light harvesting systems[55,56] and may be critical for efficient energy storage by bathorhodopsin. One possible sequence is as follows: Upon photon absorption, the chromophore begins to isomerize and impulsively drives an immediate localized, nonrandom protein response. After ~200 fs, an all-trans chromophore is completely formed; however, the chromophore is twisted due to the presence of binding pocket residues that are unable to respond further to the new chromophore structure. The highly energetic protein−chromophore complex then thermalizes over a relatively long (>20 ps) time scale. During this time, energy is transferred from the strained chromophore and the local residues it interacts with to more broadly distributed and lower frequency protein modes, ultimately resulting in diffusive protein motion which produces a planar lumi intermediate as well as the driving force for protein conformational changes.

Protein environments are designed to provide optimal reaction efficiency. In rhodopsin, a localized region of the highly specific protein binding pocket responds impulsively to the ballistic, ultrafast isomerization of the chromophore thereby permitting the isomerization reaction to occur efficiently in a tight and specific binding pocket in a *very* short period of time. However, other more delocalized protein degrees of freedom remain relatively static on the same time scale in order to efficiently store energy. These spatial and temporal separations of protein response to photoisomerization may be critical for the primary events in vision and may also be general characteristics of energy transduction systems.

## Summary

Our results provide the first structural snapshots of the initial room-temperature intermediates in the photochemistry of vision (Figure 11). Consistent with previous studies, the primary event in vision is an 11-cis to all-trans photoisomerization which is *complete* in 200 fs. Until now, the structure of the chromophore in the primary photoproduct, photorhodopsin, was unknown. Our picosecond time-resolved resonance Raman spectra indicate that photorhodopsin contains a vibrationally hot, all-trans, distorted chromophore within 200 fs of its formation. The photorhodopsin-to-bathorhodopsin transition occurs with a time constant of ~3 ps and is due to chromophore thermalization and vibrational cooling, along with some structural relaxation. Therefore, it appears that bathorhodopsin is the first true thermally relaxed intermediate in the rhodopsin photocycle. Photorhodopsin and bathorhodopsin are essentially structurally equivalent: the similarity of the fingerprint modes, the presence of intense HOOP modes, and the constancy of the 920 $cm^{-1}$ mode indicate that both species contain a highly strained, all-trans chromophore whose interaction with Glu113 remains unchanged during the transition. Finally, the striking correspondence between the room-temperature, ps time-resolved vibrational structure of photorhodopsin/bathorhodopsin and that of the low-temperature trapped primary photoproduct suggests that impulsively driven protein residue motion is a critical component of the reaction coordinate.

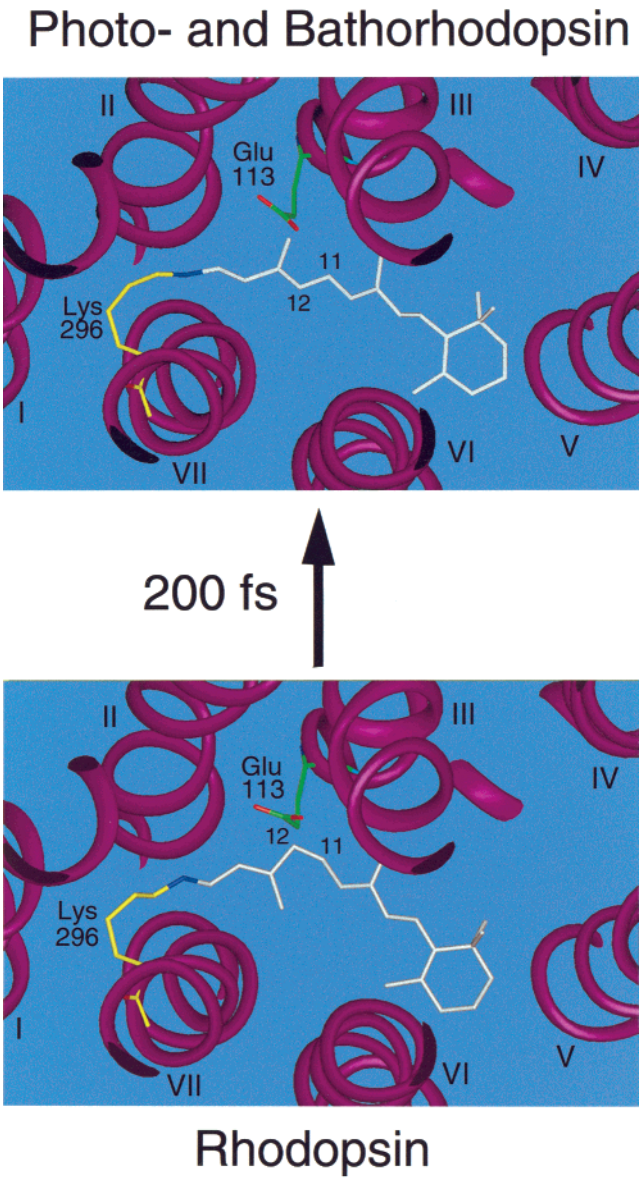


**Figure 11.** Model of the retinal binding site in rhodopsin illustrating the structural changes in the primary event. The 11-cis to all-trans photoisomerization reaction in rhodopsin is complete in 200 fs and is accompanied by impulsively driven, localized protein motion. The lack of any global motion may be important for the energy storage mechanism. The chromophore in photorhodopsin is twisted 20° in the same direction about the $C_8-C_9$, $C_{10}-C_{11}$, $C_{12}-C_{13}$, and $C_{14}-C_{15}$ bonds in order to explain the resonance enhancement of the bathorhodopsin HOOP modes.[42] The $C_{12}-Glu113$ distance is ~3 Å in both rhodopsin and its photoproduct.[50] The absolute twists around the $C_{12}-C_{13}$ bond of the chromophore in rhodopsin and photorhodopsin are consistent with an enantioselective binding study.[52] (Adapted from ref 63.)

**Note Added in Proof.** A high resolution crystal structure of rhodopsin has been published[64] since the submission of this manuscript.

**Acknowledgment.** We thank Michael Tauber and Gerd Kochendoerfer for helpful discussions and critical reading of the manuscript and Kevin Gaab and Larry Shiow for expert assistance in rhodopsin preparation. D.M. is supported by a National Science Foundation Graduate Fellowship. L.Z. is

recipient of a National Institutes of Health Postdoctoral Fellowship (EY06810). This work was supported by grants from the National Institutes of Health (EY02051) and the National Science Foundation (CHE-9801651) to R.M.

## References and Notes

(1) Fleming, G. R.; van Grondelle, R. *Curr. Opin. Struct. Biol.* **1997**, *7*, 738−748.

(2) Genick, U.; Borgstahl, G.; Kingman, N.; Zhong, R.; Pradervand, C.; Burke, P.; Srajer, V.; Teng, T.-Y.; Schildkamp, W.; Mcree, D.; Moffat, K.; Getzoff, E. *Science* **1997**, *275*, 1471−1475.

(3) Hoff, W. D.; Xie, A.; van Stokkum, I. H. M.; Tang, X.-J.; Gural, J.; Kroon, A. R.; Hellingwerf, K. J. *Biochemistry* **1999**, *38*, 1009−1017.

(4) Haupts, U.; Tittor, J.; Oesterhelt, D. *Annu. Rev. Biophys. Biomol. Struct.* **1999**, *28*, 367−399.

(5) Kochendoerfer, G. G.; Mathies, R. A. *Isr. J. Chem.* **1995**, *35*, 211−226.

(6) Mathies, R.; Lugtenburg, J. The Primary Photoreaction of Rhodopsin. In *Handbook of Biological Physics*; 2000. In press.

(7) Hamm, P.; Zurek, M.; Mantele, W.; Meyer, M.; Scheer, H.; Zinth, W. *Proc. Natl. Acad. Sci. U.S.A.* **1995**, *92*, 1826−1830.

(8) Locke, B.; Diller, R.; Hochstrasser, R. M. Ultrafast Infrared Spectroscopy and Protein Dynamics. In *Biomolecular Spectroscopy, Part B*; Clark, R. J. H., Hester, R. E., Eds.; John Wiley and Sons Ltd: New York, 1993; Vol. 21, pp 1−47.

(9) Petrich, J. W.; Martin, J. L.; Houde, D.; Poyart, C.; Orszag, A. *Biochemistry* **1987**, *26*, 7914−7923.

(10) Franzen, S.; Bohn, B.; Poyart, C.; Martin, J. L. *Biochemistry* **1995**, *34*, 1224−1237.

(11) Doig, S. J.; Reid, P. J.; Mathies, R. A. *J. Phys. Chem.* **1991**, *95*, 6372−6379.

(12) Mizutani, Y.; Kitagawa, T. *Science* **1997**, *278*, 443−446.

(13) Song, L.; El-Sayed, M. A. *J. Am. Chem. Soc.* **1998**, *120*, 8889−8890.

(14) Hayward, G.; Carlsen, W.; Siegman, A.; Stryer, L. *Science* **1981**, *211*, 942−944.

(15) Schoenlein, R. W.; Peteanu, L. A.; Mathies, R. A.; Shank, C. V. *Science* **1991**, *254*, 412−415.

(16) Peteanu, L. A.; Schoenlein, R. W.; Wang, Q.; Mathies, R. A.; Shank, C. V. *Proc. Natl. Acad. Sci. U.S.A.* **1993**, *90*, 11762−11766.

(17) Kandori, H.; Shichida, Y.; Yoshizawa, T. *Biophys. J.* **1989**, *56*, 453−457.

(18) Popp, A.; Ujj, L.; Atkinson, G. H. *J. Phys. Chem.* **1995**, *99*, 10043−10045.

(19) Green, B. H.; Monger, T. G.; Alfano, R. R.; Aton, B.; Callender, R. H. *Nature* **1977**, *269*, 179−180.

(20) Yan, M.; Manor, D.; Weng, G.; Chao, H.; Rothberg, L.; Jedju, T. M.; Alfano, R. R.; Callender, R. H. *Proc. Natl. Acad. Sci. U.S.A.* **1991**, *88*, 9809−9812.

(21) Kandori, H.; Matuoka, S.; Shichida, Y.; Yoshizawa, T.; Ito, M.; Tsukida, K.; Balogh-Nair, V.; Nakanishi, K. *Biochemistry* **1989**, *28*, 6460−6467.

(22) Mizukami, T.; Kandori, H.; Shichida, Y.; Chen, A.-H.; Derguini, F.; Caldwell, C. G.; Bigge, C. F.; Nakanishi, K.; Yoshizawa, T. *Proc. Natl. Acad. Sci. U.S.A.* **1993**, *90*, 4072−4076.

(23) Jager, F.; Ujj, L.; Atkinson, G. H. *J. Am. Chem. Soc.* **1997**, *119*, 12610−12618.

(24) Palings, I.; Pardoen, J. A.; van den Berg, E.; Winkel, C.; Lugtenburg, J.; Mathies, R. A. *Biochemistry* **1987**, *26*, 2544−2556.

(25) Applebury, M. L.; Zuckerman, D. M.; Lamola, A. A.; Jovin, T. M. *Biochemistry* **1974**, *13*, 3448−3458.

(26) Zhu, L.; Kim, J.; Mathies, R. A. *J. Raman Spectrosc.* **1999**, *30*, 777−783.

(27) Mathies, R.; Oseroff, A. R.; Stryer, L. *Proc. Natl. Acad. Sci. U.S.A.* **1976**, *73*, 1−5.

(28) Kochendoerfer, G. G.; Mathies, R. A. *J. Phys. Chem.* **1996**, *100*, 14526−14532.

(29) Lin, S. W.; Groesbeek, M.; van der Hoef, I.; Verdegem, P.; Lugtenburg, J.; Mathies, R. A. *J. Phys. Chem. B* **1998**, *102*, 2787−2806.

(30) Smith, S. O.; Myers, A. B.; Mathies, R. A.; Pardoen, J. A.; Winkel, C.; van den Berg, E. M. M.; Lugtenburg, J. *Biophys. J.* **1985**, *47*, 653−664.

(31) Kochendoerfer, G. G.; Verdegem, P. J. E.; van der Hoef, I.; Lugtenburg, J.; Mathies, R. A. *Biochemistry* **1996**, *35*, 16230−16240.

(32) Wang, Q.; Kochendoerfer, G. G.; Schoenlein, R. W.; Verdegem, P. J. E.; Lugtenburg, J.; Mathies, R. A.; Shank, C. V. *J. Phys. Chem.* **1996**, *100*, 17388−17394.

(33) Schoenlein, R. W.; Peteanu, L. A.; Wang, Q.; Mathies, R. A.; Shank, C. V. *J. Phys. Chem.* **1993**, *97*, 12087−12092.

(34) Garavelli, M.; Celani, P.; Bernardi, F.; Robb, M. A.; Olivucci, M. *J. Am. Chem. Soc.* **1997**, *119*, 6891−6901.

(35) Vreven, T.; Bernardi, F.; Garavelli, M.; Olivucci, M.; Robb, M. A.; Schlegel, H. B. *J. Am. Chem. Soc.* **1997**, *119*, 12687−12688.

(36) Garavelli, M.; Vreven, T.; Celani, P.; Bernardi, F.; Robb, M. A.; Olivucci, M. *J. Am. Chem. Soc.* **1998**, *120*, 1285−1288.

(37) Wang, Q.; Schoenlein, R. W.; Peteanu, L. A.; Mathies, R. A.; Shank, C. V. *Science* **1994**, *266*, 422−424.

(38) Callender, R.; Honig, B. *Annu. Rev. Biophys. Bioeng.* **1977**, *6*, 33−55.

(39) Eyring, G.; Curry, B.; Broek, A.; Lugtenburg, J.; Mathies, R. *Biochemistry* **1982**, *21*, 384−393.

(40) Eyring, G.; Curry, B.; Mathies, R.; Fransen, R.; Palings, I.; Lugtenburg, J. *Biochemistry* **1980**, *19*, 2410−2418.

(41) Jager, F.; Lou, J.; Nakanishi, K.; Ujj, L.; Atkinson, G. H. *J. Am. Chem. Soc.* **1998**, *120*, 3739−3747.

(42) Palings, I.; van den Berg, E. M. M.; Lugtenburg, J.; Mathies, R. A. *Biochemistry* **1989**, *28*, 1498−1507.

(43) Kakitani, H.; Kakitani, T.; Rodman, H.; Honig, B. *Photochem. Photobiol.* **1985**, *41*, 471−479.

(44) Smith, S. O.; Courtin, J.; de Groot, H. J. M.; Gebhard, R.; Lugtenburg, J. *Biochemistry* **1991**, *30*, 7409−7415.

(45) Buda, F.; de Groot, H. J. M.; Bifone, A. *Physical Review Lett.* **1996**, *77*, 4474−4477.

(46) La Penna, G.; Buda, F.; Bifone, A.; de Groot, H. J. M. *Chem. Phys. Lett.* **1998**, *294*, 447−453.

(47) Bifone, A.; de Groot, H. J. M.; Buda, F. *Pure Appl. Chem.* **1997**, *69*, 2105−2110.

(48) Reid, P. J.; Wickham, S. D.; Mathies, R. A. *J. Phys. Chem.* **1992**, *96*, 5720−5724.

(49) Shreve, A. P.; Mathies, R. A. *J. Phys. Chem.* **1995**, *99*, 7285−7299.

(50) Han, M.; Smith, S. O. *Biochemistry* **1995**, *34*, 1425−1432.

(51) Kochendoerfer, G. G.; Lin, S. W.; Sakmar, T. P.; Mathies, R. A. *T.I.B.S.* **1999**, *24*, 300−305.

(52) Lou, J.; Hashimoto, M.; Berova, N.; Nakanishi, K. *Org. Lett.* **1999**, *1*, 51−54.

(53) Yoshizawa, T.; Horiuchi, S. Studies on Intermediates of Visual Pigments by Absorption Spectra at Liquid Helium Temperature and Circular Dichroism at Low Temperatures. In *Biochemistry and Physiology of Visual Pigments*; Langer, H., Ed.; Springer-Verlag: 1973; pp 69−81.

(54) Aton, B.; Callender, R. H.; Honig, B. *Nature* **1978**, *273*, 784−786.

(55) Homoelle, B. J.; Edington, M. D.; Diffey, W. M.; Beck, W. F. *J. Phys. Chem. B* **1998**, *102*, 3044−3052.

(56) Riter, R. R.; Edington, M. D.; Beck, W. F. *J. Phys. Chem.* **1996**, *100*, 14198−14205.

(57) Siebert, F.; Mantele, W.; Gerwert, K. *Eur. J. Biochem.* **1983**, *136*, 119−127.

(58) Bagley, K. A.; Balogh-Nair, V.; Croteau, A. A.; Dollinger, G.; Ebrey, T. G.; Eisenstein, L.; Hong, M. K.; Nakanishi, K.; Vittitow, J. *Biochemistry* **1985**, *24*, 6055−6071.

(59) DeGrip, W. J.; Gray, D.; Gillespie, J.; Bovee, P. H. M.; van den Berg, E. M. M.; Lugtenburg, J.; Rothschild, K. J. *Photochem. Photobiol.* **1988**, *48*, 497−504.

(60) Kandori, H.; Maeda, A. *Biochemistry* **1995**, *34*, 14220−14229.

(61) Nagata, T.; Terakita, A.; Kandori, H.; Kojima, D.; Shichida, Y.; Maeda, A. *Biochemistry* **1997**, *36*, 6164−6170.

(62) Nagata, T.; Tarakita, A.; Kandori, H.; Shichida, Y.; Maeda, A. *Biochemistry* **1998**, *37*, 17216−17222.

(63) Kochendoerfer, G. G.; Wang, Z.; Oprian, D. D.; Mathies, R. A. *Biochemistry* **1997**, *36*, 6577−6587.

(64) Palczewski, K.; Kumasaka, T.; Hori, T.; Behnke, C. A.; Motoshima, H.; Fox, B. A.; LeTrong, I.; Teller, D. C.; Okada, T.; Stenkamp, R. E.; Yamamoto, M.; Miyano, M. *Science* **2000**, *289*, 739−745.